Journal of Theoretical and Computational Acoustics

ACOUSTIC RADIATION CHARACTERISTICS OF A FORCED VIBRATING ELASTIC PANEL UNDER THERMAL ENVIRONMENTS

MANUEL GASCÓN-PÉREZ
Escuela Técnica Superior de Ingeniería Aeronáutica y del Espacio
Universidad Politécnica de Madrid
28040 Madrid, Spain
manuel.gascon@upm.es
orcid.org/0000-0003-4593-730X

Received
Revised

This paper presents the thermo-acoustic frequency response of an un-baffled rectangular panel subjected to an external excitation load. A boundary element method BEM has been employed taking into account the Kirchhoff-Helmholtz K-H integral equation for the acoustic pressure and with the fluid-plate interface boundary condition the acoustic pressure jump over the panel is calculated. The thermal effects are considered regarding in the form of a uniform increment of temperature of the panel and are analysed in order to prevent the buckling phenomena. The excitation force considered is in the form of a concentrated load at some point of the panel and the deformation modes correspond to the vacuum case. Applying a collocation method for the panel equation, a frequency transfer function is obtained that relates the deflexion of the panel with the applied load . The effect of several geometric parameters, different thermal loads and location of the load applied on the acoustic radiated power and the acoustic efficiency spectrum are evaluated. Furthermore, the influence of the excitation frequency on the sound directivity is evaluated. The verification of the method is proven with other works.

Keywords**:** rectangular panel; thermo-acoustic behaviour; fluid-structure interaction; acoustic radiation; boundary element method**.**

1. Introduction

Interaction of structures with fluid are present in a wide variety of technological applications in the fields of aerospace, civil or naval engineering. Prediction of sound radiation by these vibrating structures submerged in fluid is of great importance to control noise generation. Sound power and radiation efficiency (or radiation ability) are the two parameters usually employed to investigate the radiation characteristics of these structures. There are many works in this regard, for the case of unbaffled plates as is the case of the present study, the works of Atalalla et al [1] where the acoustic radiation characteristics of an unbaffled vibrating plate with general elastic boundary conditions is analyzed, or Laulagnet [2] that study of the sound radiation of a simply supported unbaffled plate, and for baffled plates the work of Berry et al [3] that analyze the sound radiation of rectangular plates with different boundary conditions. The BEM is widely used for the analysis of sound radiation for reasons of time and cost of computation. In some specific engineering applications light structures are employed and the low weight results in high level of noise which is related with the magnitude and frequency of structural vibrations. It is important for the designer to minimize the radiated noise that can affect the mechanical behavior of the structures and might be harmful to human beings working for example in space vehicles, Wilby [4]. Different parameters have an important influence on the acoustic radiation performance of the structures, such as type and location of excitation load, material and geometric properties of these structures as well as thermal and hygroscopic environment. This thermal environment, studied in early literature regarding structure dynamic behaviour date from 1950s as in Boley et. al [5], or the investigation of Kim [6] on the vibration of functionally graded materials (FGM) of plates under thermal environments. Thermal stresses have an important influence on the dynamic and stiffness characteristics of structures employed in space vehicle applications due to the heating solar radiation and in the case of very light structures the surrounding fluid as the case of air in earth test or essays has an important influence on the vibration behavior. Panels structures are employed in the construction of airplanes and space vehicles and must not only meet the structural requirements, but also minimized the radiated noise and provide insulation from the surrounding environment, so in the design of airframe structures plays an important role the investigation of the vibro-acoustic response for an optimal behavior. The acoustic properties can be used for estimation of material properties such in FGM of the structure, see Liu et al [7], non-destructive evaluation, see Iyer et al [8], structural health monitoring , see Meo et al [9] and acoustic imaging, see Maev [10].

Jeyaraj et al. [11] employed a combination of finite and boundary element methods investigating the vibro-acoustic behaviour of isotropic and composite plates under thermal environment. Geng and Li [12] studied the dynamic and acoustic radiation characteristics of a flat isotropic plate under thermal environments, showing that thermal loads influence on the stress state and the change in the natural frequencies, mainly the fundamental frequency.

Chandra et al [13] study the vibroacoustic response and sound transmission loss of functionally graded plates under various types of load. The work of Yang et al [14] where the sound radiation of FGM in thermal environment is analysed.

Li and Yu [15] analysed the vibration and acoustic response of sandwich panels under thermal environments, taking into account the Rayleigh integral for the pressure distribution and analogously the works of Li et al [16] and Liu & Li [17]. Recently, many works made by Sharma et al [18,19,20] regarding the acoustic radiation characteristics of baffled and unbaffled flat and curved composite vibrating structures with various support boundary conditions under harmonic excitations, considering thermal and moisture environments.

Moreover, there are currently some interesting technological applications in the field of acoustics related with passive and active control acoustics regarding fluid-structure interaction problems, for example that of acoustic black holes, see Cao et al [21], or acoustic metamaterials, see Kumar and Lee [22], respectively.

Some works, Sobhy [23] and Zhou [24], study the case of functionally graded materials employed in the construction of the structure and not as in the present work where an homogeneous composition and temperature of the panel is considered.

The work of Gascón-Pérez [25] where the thermo-acoustic behaviour of a free vibrating rectangular panel is analyzed by the application of a BEM as in the present study so it can be conclude the validation of the present work.

The acoustic radiation behaviour of a simply supported rectangular panel is analyzed in this paper with a BEM and using the K-H integral equation, considering the influence of several parameters and the temperature on its forced vibration response.

2. Analytical Formulation

The thermo-acoustic response of a rectangular panel with thermal stress due only to a uniform increment of temperature and fully immersed in the fluid and exited by a forcing load f_0 located at x_0, y_0 position, is governed by the equation, see Wang et al. [26] and Boley et al. [27]:

$$D\nabla^4 u(x,y,t) + \frac{N_T}{1-\nu}\Delta u(x,y,t) + \rho_m t_h \frac{\partial^2 u}{\partial t^2} = \delta p(x,y,t) + \delta f_0(x,y,t) \tag{2.1}$$

With u the normal displacement of the plate, $D=\dfrac{E\cdot t_h^{\;3}}{12\left(1-\nu^2\right)}$ the flexural rigidity, E the Young's modulus of the material, t_h the panel thickness, ν the Poisson's ratio and ρ_m the material density of the panel.

N_T is a thermal parameter regarding the in-plane forces of the panel associated to the thermal loads that is expressed as:

$$N_T = \alpha\, t_h E\, \Theta \tag{2.2}$$

Being α the thermal expansion coefficient of the panel material and Θ the uniform temperature (increment of temperature) of the panel, where it has been considered the zero value for the reference temperature of the panel. All material properties are considered constant, that is, independent of temperature.

And $\delta f(x,y,t)$ is the harmonic excitation force per unit area expressed as a Dirac-delta located at x_0, y_0 position associated to a load f_0 of 1N so that $\delta f_0(x,y,t)=\delta \tilde{f}_0(x,y)\cdot e^{-i\omega t}$

And $$f_0 = \iint_{S_p} \delta \tilde{f}_0\left(x-x_0, y-y_0\right) dx\, dy \tag{2.3}$$

Fig.1 represents the configuration of the panel submerged in an infinite fluid at rest.

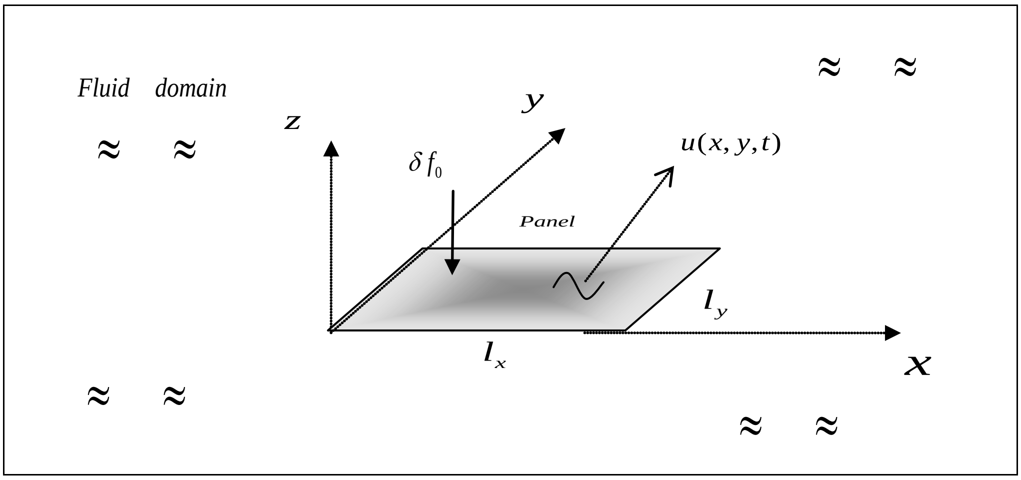

Fig. 1. Scheme of a rectangular panel surrounded by fluid and its geometric characteristics

The acoustic action over the panel due to the fluid is the pressure jump δp between its upper and lower sides.

Considering harmonic motion for both the fluid and structure, the solution takes this form:

$$u(x,y,t)=\tilde{u}(x,y)\cdot e^{-i\omega t} \text{ and } p(x,y,z,t)=\tilde{p}(x,y,z)\cdot e^{-i\omega t} \tag{2.4}$$

The deflection of the panel coupled with fluid is expressed in series of the deformation modes in vacuum:

$$\tilde{u}(x,y)=\sum_m\sum_n \tilde{u}_m^n(x,y)=\sum_m\sum_n \varphi_m^n(x,y)\cdot \overline{u}_m^n \tag{2.5}$$

Where $\overline{u}_m^n$ represent the weight coefficient associated to each mode, that takes into account the effect of the acoustic medium.

The modes in vacuum $\varphi_m^n(x,y)$ for a simply supported panel, have the general expression Wang [26].

$$\varphi_m^n(x,y) = sin\frac{m\pi x}{l_x}\cdot sin\frac{n\pi y}{l_y} \tag{2.6}$$

Being m,n integer numbers associated to the number of nodes of null deflection.
Expanding in series of the deformation modes in vacuum the concentrated load:

$$\delta\tilde{f}_0(x,y) = \sum_m\sum_n \overline{f}_m^n\cdot\varphi_m^n(x,y) \tag{2.7}$$

Where the coefficients have the expression:

$$\overline{f}_m^n = \frac{4}{l_xl_y}\iint_{S_p}\delta\tilde{f}_0(x-x_0,y-y_0)\cdot\varphi_m^n(x,y)dxdy = \frac{4}{l_xl_y}f_0\cdot\varphi_m^n(x_0,y_0) \tag{2.8}$$

Considering the wave equation for the fluid pressure, and the assumption of harmonic motion, the Helmholtz's equation is deduced:

$$\Delta\tilde{p} + k^2\tilde{p} = 0 \tag{2.9}$$

Where $k = \frac{\omega}{a_\infty}$ is the wave number, being a_∞, the sound speed

And considering the interface boundary condition at $z = 0$ and $0 < x < l_x$, $0 < y < l_y$ of the momentum equation:

$$\left.\frac{\partial\tilde{p}(x,y,z)}{\partial z}\right|_{z=0} = \rho_\infty\omega^2\tilde{u}(x,y) = \rho_\infty\omega^2\sum_n\sum_m\varphi_m^n(x,y)\cdot\overline{u}_m^n \tag{2.10}$$

Being ρ_∞, the fluid density

2.1 Buckling Temperature

The buckling temperature is calculated finding the nonzero solutions for the thermo-elastic static problem defined by the equation (2.1) considering only the first two terms i.e. the rigidity and thermal components with no time dependence. Taking into account the deformation equation (2.4) and the expression for the thermal parameter, equation (2.2), it is deduced the critical buckling temperature corresponding to the fundamental mode, that is considered to prevent any excess thermal loading in the analysis of the results:

$$\Delta T_{cr} = \Theta_{cr} = \frac{{t_h}^2\pi^2}{12(1+\nu)\alpha}\left[\left(\frac{1}{l_x}\right)^2+\left(\frac{1}{l_y}\right)^2\right] \tag{2.11}$$

2.2 Calculus of the pressure jump over the plate

First is considered the K-H integral equation that relates the pressure field with the pressure jump over the panel, see Junger [28], Crocker [29], Fahy [30].

$$\tilde{p}(x,y,z) = -\frac{1}{4\pi}\iint_{S_p}\delta\tilde{p}(\xi,\eta)\frac{\partial}{\partial z}\left(\frac{e^{ikR}}{R}\right)d\xi d\eta \tag{2.12}$$

Being R, the distance between the field and source points and S_p the panel surface.

Considering the boundary condition (2.10), and by applying a collocation method, the following equation for the pressure jump is obtained associated to each mode:

$$\left\{\delta P_m^n(\overline{\xi}_r,\overline{\eta}_s)\right\} = \rho_\infty \omega^2 \left[\Gamma_{ij}^{rs}\right]^{-1} \left\{\varphi_m^n(x_i,y_j)\right\} \overline{u}_m^n \quad (2.13)$$

Where the matrix is obtained by integration of the kernel Υ on each rectangular element of the panel

$$\Gamma_{ij}^{rs} = -\frac{1}{4\pi} \int_{\xi_r}^{\xi_{r+1}} \int_{\eta_s}^{\eta_{s+1}} \Upsilon\left(x_i-\xi, y_i-\eta, 0, k\right) d\xi \, d\eta \quad (2.14)$$

Being $\Upsilon = \left.\dfrac{\partial^2}{\partial z^2}\left(\dfrac{e^{ikR}}{R}\right)\right|_{z=0}$

Special care must be taken when evaluating the integral and the field and source points coincides, so a principal value is taken, see Roussos [31]. More details can be found in Gascón-Pérez [32]

2.3 Calculus of the frequency response of the panel

Applying the generalized work equation of the mn modal forces of the panel equation associated to the uv modal panel deflection and making variation of the modal numbers $m,n,u,v = 1,2,..........,N$, the following system is obtained, for the calculus of the deformation weight coefficients in relation to the applied load with an associated transfer function:

$$\left[\left[K\right] - \omega^2\left(\left[M\right] + \left[M_F\right]\right)\right]\left\{\overline{u}\right\} = \left[\Phi\right]\left\{\overline{f}\right\} \quad (2.15)$$

Where the coefficients of these matrices are expressed:

$$K_{mu}^{nv} = D\left\lfloor \Delta^2 \varphi_m^n \right\rfloor \left[\Delta S\right]\left\{\varphi_u^v\right\} + \frac{N_T}{1-\nu}\left\lfloor \Delta \varphi_m^n \right\rfloor \left[\Delta S\right]\left\{\varphi_u^v\right\} \quad (2.16.1)$$

$$M_{mu}^{nv} = \rho_m t_h \left\lfloor \varphi_m^n \right\rfloor \left[\Delta S\right]\left\{\varphi_u^v\right\} \quad (2.16.2)$$

$$M_{Fmu}^{nv} = \rho_\infty \left\lfloor \varphi_m^n \right\rfloor \left[\left[\Gamma\right]^{-1}\right]^T \left[\Delta S\right]\left\{\varphi_u^v\right\} \quad (2.16.3)$$

$$\Phi_{mu}^{nv} = \left\lfloor \varphi_m^n \right\rfloor \left[\Delta S\right]\left\{\varphi_u^v\right\} \quad (2.16.4)$$

Where $\left[\Delta S\right]$ is the matrix associated to the panel surface, is a diagonal matrix whose elements correspond to the surface of the discrete rectangular element in which is divided the total rectangular surface of the panel.

And finally solving the deformation weight coefficients as function of the applied load:

$$\left\{\overline{u}\right\} = \left[\ \mathrm{T}\ \right]\left\{\overline{f}\right\} \quad (2.17)$$

Where the transfer function has this expression:

$$\left[\ \mathrm{T}\ \right] = \frac{\left[\Phi\right]}{\left[\ \left[K\right] - \omega^2\left(\left[M\right] + \left[M_F\right]\right)\ \right]} \quad (2.18)$$

Because the fluid mass matrix depends of the wave number k, the solution for the calculus of the natural frequencies is obtained by an iteration procedure in an easy way due to the fast convergence. The iteration procedure is applied to obtain the natural vibration frequencies one by one. For a given natural frequency, an initial value of this frequency and also the associated wave number is assumed, and iteration in only a few steps (3 or 4) is sufficient to obtain the final frequency result. For each of the rest of the natural frequencies the procedure is analogous. The modes of the coupled fluid-structure can be obtained taking into account the eigenvector $\{\bar{u}\}$ and the corresponding modes in vacuum.

2.4 Calculus of the acoustic power and radiation efficiency

The acoustic power is calculated from the following expression:

$$P_a = \mathrm{Re}\left\{ \iint_{S_p} \delta p \cdot \dot{u} \cdot dS \right\} \tag{2.19}$$

And the acoustic radiation efficiency defined as:

$$\sigma = \frac{P_a}{\rho_\infty a_\infty S_p \left\langle \dot{u}^2 \right\rangle} \tag{2.20}$$

Being $\left\langle \dot{u}^2 \right\rangle$ the quadratic medium panel velocity that is calculated as:

$$\left\langle \dot{u}^2 \right\rangle = \frac{1}{S_p} \iint_{S_p} \left| \dot{u} \right|^2 \cdot dS \tag{2.21}$$

These expressions are interpreted after average integration over the time period for harmonic motion.

Taking into account the expressions for the pressure jump (2.13) and plate deflexion (velocity) (2.5), can be deduced the acoustic power and the radiation efficiency in the following form:

$$P_a = \mathrm{Re}\left\{ -i\omega^3 \lfloor \bar{\mathrm{u}} \rfloor [\mathrm{M_F}] \{\bar{\mathrm{u}}\} \right\} \tag{2.22}$$

$$\sigma = \mathrm{Re}\left\{ -i\omega \frac{\lfloor \bar{\mathrm{u}} \rfloor [\mathrm{M_F}] \{\bar{\mathrm{u}}\}}{\rho_\infty a_\infty \lfloor \bar{\mathrm{u}} \rfloor [\Phi] \{\bar{\mathrm{u}}\}} \right\} \tag{2.23}$$

In particular, the modal radiation efficiency associated to the mn mode is expressed as:

$$\sigma_m^n = \mathrm{Re}\left\{ -ik \frac{\lfloor \varphi_m^n \rfloor \left[[\Gamma]^{-1} \right]^T [\Delta S] \{\varphi_m^n\}}{\lfloor \varphi_m^n \rfloor [\Delta S] \{\varphi_m^n\}} \right\} \tag{2.24}$$

2.5 Sound directivity

Directivity is important because it helps indicate how much sound will be directed towards a specific area compared to all the sound energy being generated by a source.

It is a well-known property of modern loudspeakers that sound is not radiated equally in all directions for all frequencies. The directivity of a loudspeaker describes the extent to which the acoustic power produced by the loudspeaker is biased toward a given direction.

Plates with different sizes and aspect ratios are widely used as important structural components in vehicles, airplanes, industrial machinery, buildings and bridges. They are also important components in the radiation of noise when the structures are subjected to dynamic loading. For the purpose of predicting and mitigating noise from complex structures, it is helpful to understand the sound radiation from vibrating plates; particularly common are those with rectangular shape. Two important factors that influence the radiated sound power of a vibrating plate are the spatially-averaged vibration velocity and the radiation efficiency of the plate. In addition, the sound directivity also plays an important role in determining the distribution of sound pressure for external radiation problems.

The directivity is represented in logarithmic scale of the sound pressure level SPL and is obtained with the expression $SPL = 20 \cdot \log\left(\frac{p}{p_{ref}}\right)$ being $p_{ref} = 2 \cdot 10^{-5}\ Pa$ and p is the sound pressure at a field point x, y, z obtained with the expression:

$$\tilde{p}(x,y,z) = -\frac{1}{4\pi}\iint_{S_p} \delta\tilde{p}(\xi,\eta)\cdot\lambda\left(x-\xi, y-\eta, z, k\right) d\xi d\eta \qquad (2.25)$$

Being $\lambda = \frac{\partial}{\partial z}\left(\frac{e^{ikR}}{R}\right)$

Taking into account the expression for the pressure jump over the panel, equation (2.13), finally it is obtained the acoustic pressure at the field point 0

$$\tilde{p}(x,y,z) = \lfloor \Pi \rfloor \{\overline{u}\} \qquad (2.26)$$

Where the vector $\lfloor \Pi \rfloor$ is expressed:

$$\Pi_m^n = \rho_\infty\, \omega^2 \left\lfloor \varphi_m^n \right\rfloor \left[\left[\Gamma\right]^{-1}\right]^T \{\Lambda\} \qquad (2.27)$$

And Λ is expressed as:

$$\Lambda_r^s = -\frac{1}{4\pi}\int_{\xi_r}^{\xi_{r+1}}\int_{\eta_s}^{\eta_{s+1}} \lambda\left(x-\xi, y-\eta, z, k\right) d\xi\, d\eta \qquad (2.28)$$

3. Results and discussion

A validation of the method is made comparing the results obtained by Kwak [33] for the natural frequencies of a vibrating baffled plate with surrounding water by the upper and lower sides with the present method (for which the equation (2.1) is considered without the thermal and forcing terms) and it is found a good agreement but with a slight difference depending of the mode considered, that can be due to the difference of the boundary conditions presented in the two cases (baffle or unbaffled), see Table 1. Also these results are compared with those obtained in the work of Gascón-Pérez [25] and in this case the values obtained are all the same.

Table 1. Natural frequencies (Hz) for a simply supported rectangular steel plate (in vacuum f_v and water f_l) immersed in fluid, of side lengths $l_x = 5m$, $l_y = 4m$, and thickness $t_h = 1cm$

m , n	f_v	f_l (Kwak)	f_l (present method and Gascón-Pérez)	Relative discrepancy (%)
1 , 1	2.498	0.398	0.435	8.5
1 , 2	5.422	1.093	1.171	7.1
2 , 1	7.067	1.561	1.623	3.9
2 , 2	9.991	2.468	2.503	1.4

Also for validation of this method, the results obtained by Atalla et al [1] of the radiation efficiency spectrum in dB and showed in Fig.2 for an unbaffled plate with the properties indicated in the same figure are compared with that obtained in the present method as presented in Fig. 3 (the load is applied at 25% lx, ly position), and as it can be seen there are also similarity between the curves in the two figures. It must be said that in the case of Atalla the point force is non centered but it does not gives the exact position of the load location, while in the present method the point force is applied at 25% lx, ly position, so the small differences in the graphical results presented

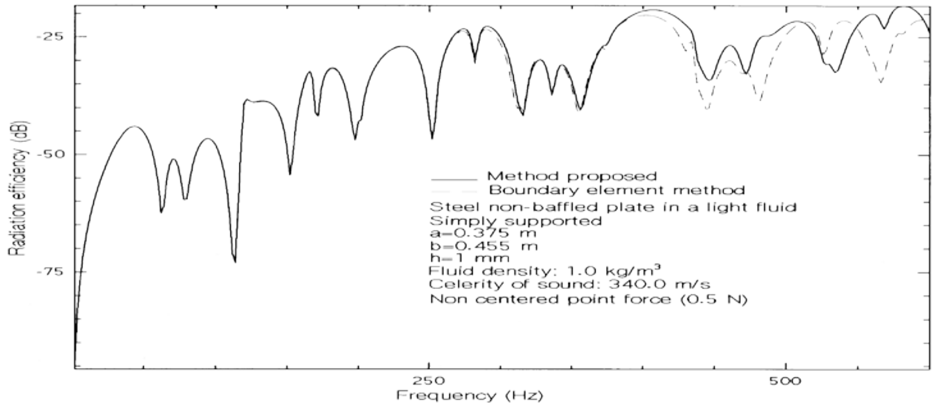

Fig.2. . Variation of the radiation efficiency with the frequency Atalalla [1]

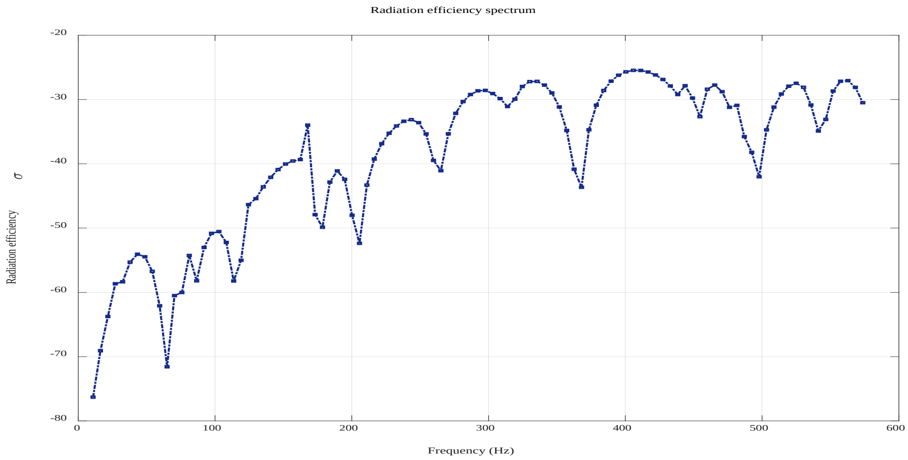

Fig. 3. Variation of the radiation efficiency with the frequency, present method

Finally regarding the validation of the method, the results obtained by Li and Li [34], for a baffled plate with fluid on one side, of the sound power level spectrum in dB and showed in Fig.4 for a rectangular steel plate of side lengths $l_x = 0.455\,m$, $l_y = 0.379m$ and thickness $t_h = 3\,mm$, excited at center position by a 1 N driving point force, are compared with that obtained in the present method as presented in Fig. 5, and as it can be seen there are similarity between the curves in the two figures, although it must be said that in the present method the plate is unbaffled and fully immersed in fluid, so the small differences in the results.

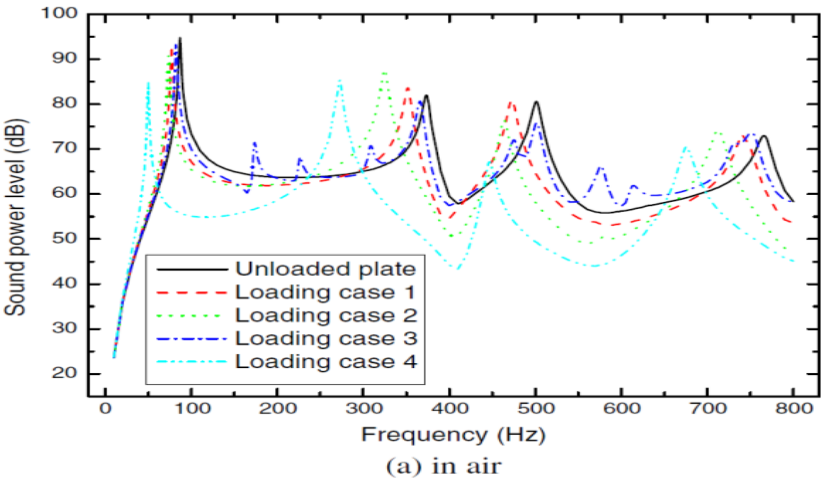

Fig. 4. Variation of the sound power level with the frequency Li & Li [34]

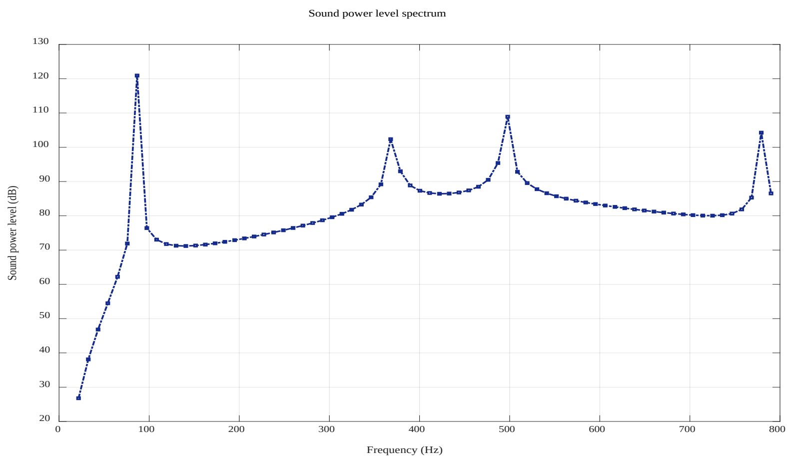

Fig. 5. Variation of the sound power level with the frequency, present method

The next results were obtained for the case of a simply supported composite rectangular panel submerged in air (compressible fluid), and the following properties are considered:

Side lengths $l_x = 2\,m$, $l_y = 1.5\,m$, thickness $t_h = 10\,mm$, material density $\rho_m = 200\,\frac{kg}{m^3}$,

Young's modulus $E = 9\,Gpa$, Poisson's ratio $\nu = 0.3$, thermal expansion coefficient $\alpha = 10^{-6}\,\frac{m}{K}$

First the critical buckling temperature Θ_{cr} is calculated with equation (2.11) in order to prevent any excess of this limit in the presented results, for the panel properties above considered, being $\Delta T_{cr} = \Theta_{cr} = 43.94\,{}^{0}C$

The acoustic power and the radiation efficiency are expressed in the following Figures in logarithmic scale as sound power level spl (dB) and radiation efficiency σ (dB) and have the expressions:

$$spl(dB) = 10\log\left(\frac{P_a}{P_{ref}}\right) \quad \text{with} \quad P_{ref} = 10^{-12} W$$

$$\sigma(dB) = 10\log(\sigma)$$

In all cases the frequency of the resonant peaks coincides with the natural frequency of vibration and the number of peaks depends on the point of application of the force applied, so that in some cases not all frequencies are excited. With the variation of the different parameters the frequency response differs from the reference condition, and the new resonant peaks correspond to the natural frequencies of the new condition, so that if the resonant frequencies decrease or increase with the variation of the parameter, the resonant peaks are also shifted to lower or higher values of the spectrum frequency.

Fig. 6 and 7 presents for the reference values of the panel, the variation of the radiation efficiency and the sound power level with the frequency. The different peaks corresponds to the resonant frequencies that coincides with the natural frequencies of vibration of the panel in contact with the fluid. Without considering the peaks, an increasing variation of the radiation efficiency with the frequency is observed in the frequency spectrum (0-250 Hz), while the sound power level initially presents an increasing variation in the range (0 – 100 Hz) and almost remains constant for higher values of the frequency

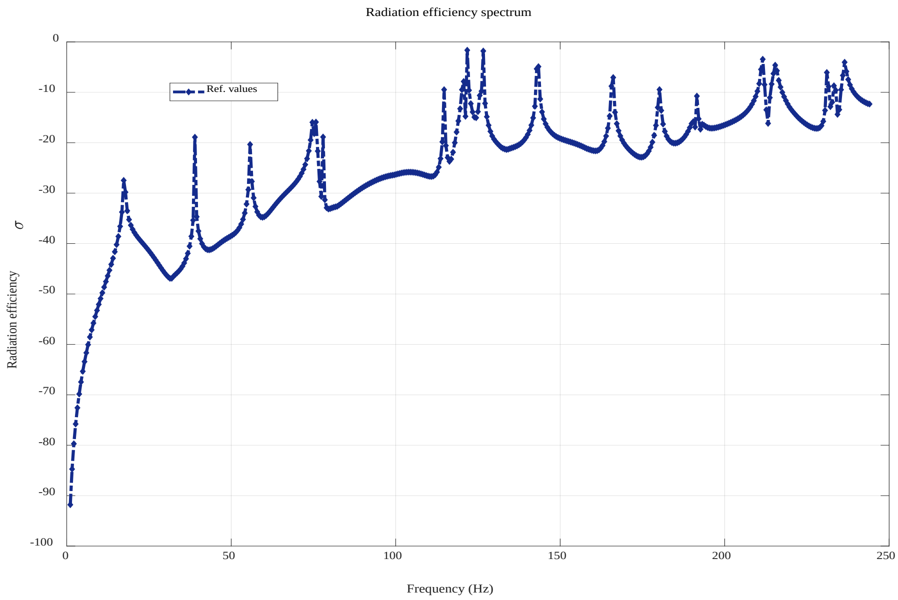

Fig. 6. Variation of the radiation efficiency with the frequency

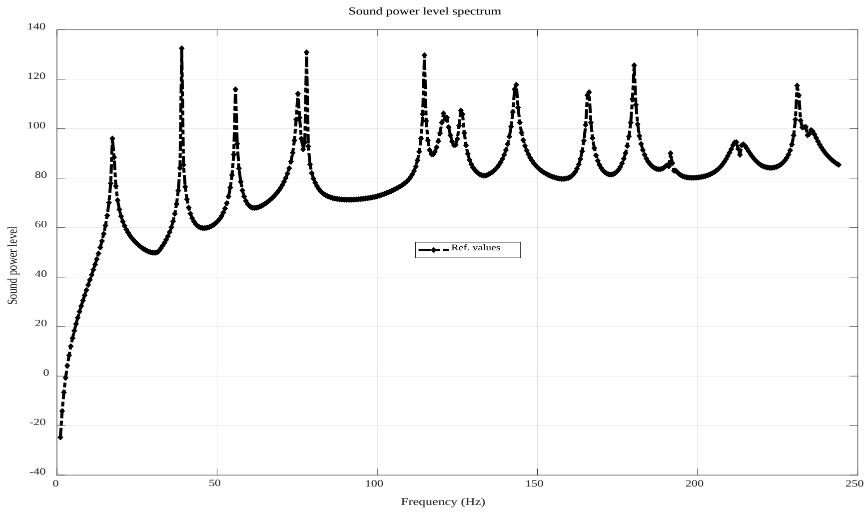

Fig. 7. Variation of the sound power level with the frequency

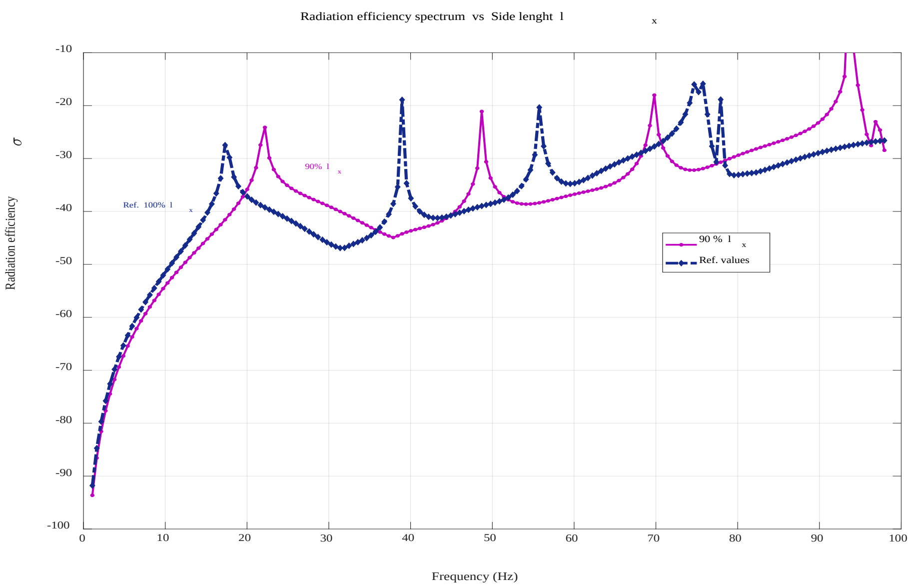

Fig. 8. Variation of the radiation efficiency with the frequency for different values of the side length

Fig. 8 and 9 presents the variation of the radiation efficiency and the sound power level with the frequency for different values of the panel dimension expressed as the side length l_x and considering constant the aspect ratio l_y / l_x. The resonant peaks are shifted to higher values of the frequency for the smaller panel ($90\% \, l_x$) compared with respect to those of the reference panel $(100\% \, l_x)$, and the frequency interval between these peaks are also greater for the smaller panel.

The radiation efficiency and the sound power level for the fundamental frequency are slightly higher the lower the value of the panel dimension.

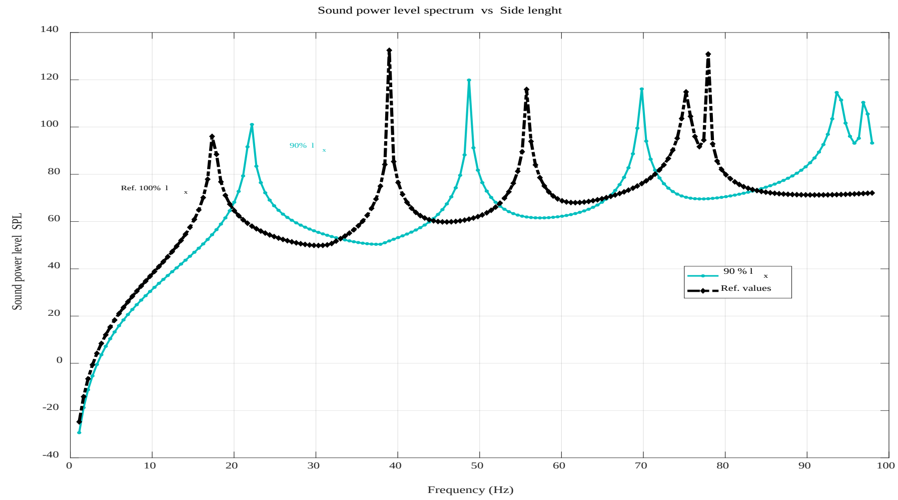

Fig. 9. Variation of the sound power level with the frequency for different values of the side length

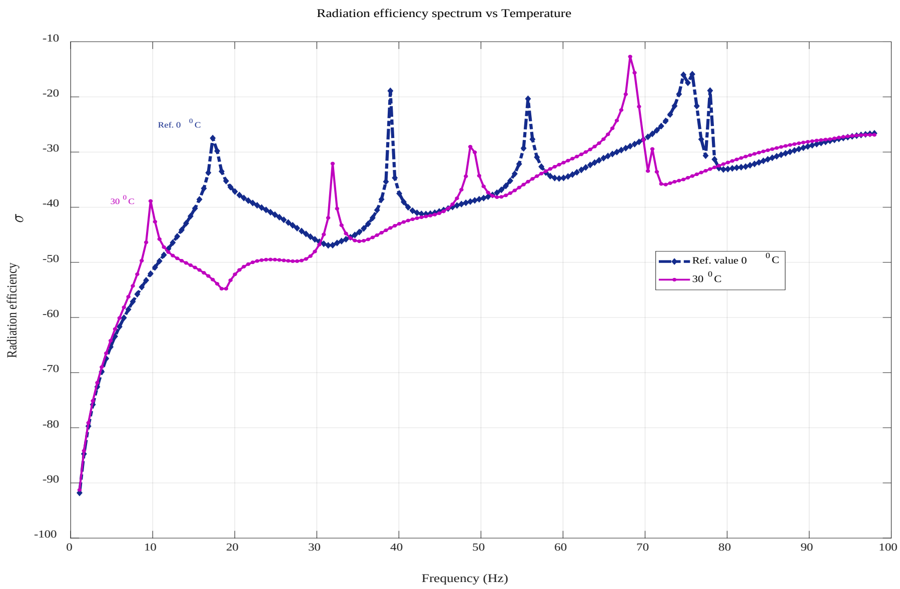

Fig. 10. Variation of the radiation efficiency with the frequency for different values of the temperature

Fig. 10 and 11 presents the variation of the radiation efficiency and the sound power level with the frequency for different values of the panel temperature $\Theta = 0^0 C$, $30^0 C$. The frequency values of the peaks are higher the lower the value of the panel temperature, but the frequency intervals between these resonant peaks remains almost constant with the temperature.. The radiation efficiency and the sound power level for the fundamental frequency are lower the higher the value of the panel temperature.

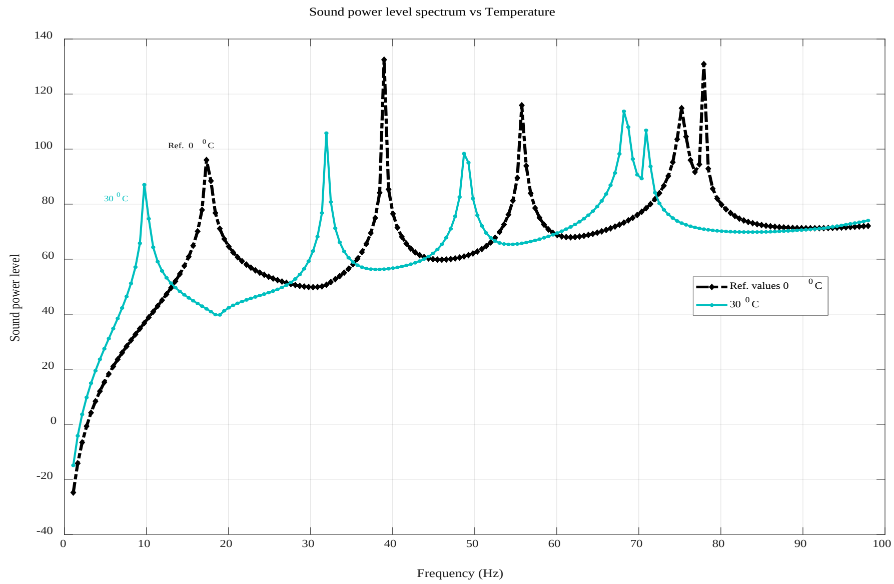

Fig. 11. Variation of the sound power level with the frequency for different values of the temperature

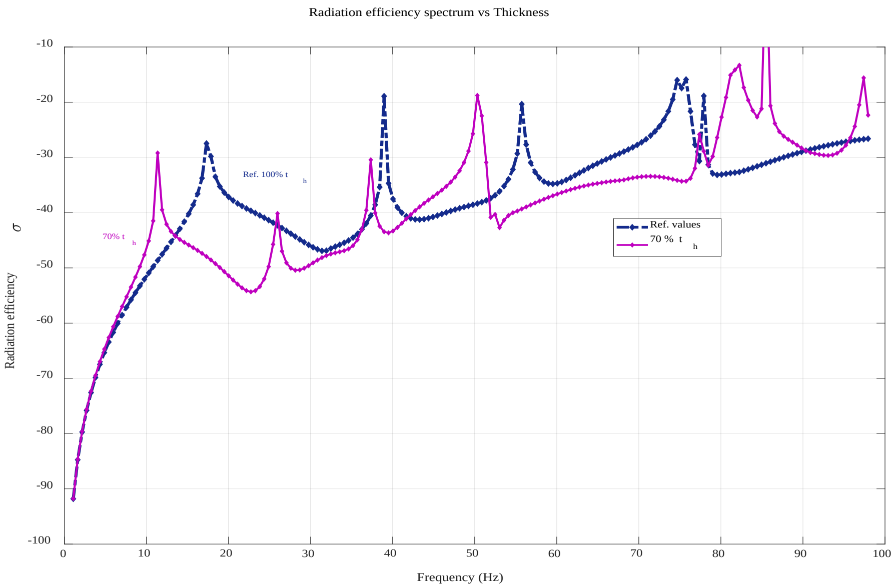

Fig. 12. Variation of the radiation efficiency with the frequency for different values of the thickness

Fig. 12 and 13 presents the variation of the radiation efficiency and the sound power level with the frequency for different values of the panel thickness. The different resonant peaks are found for lower values of the frequency as lower the value of the thickness and the frequency interval between these peaks is lower for the thinner panel. The radiation efficiency for the fundamental frequency is almost similar for both thicknesses, but the sound power level is higher for the thinner panel.

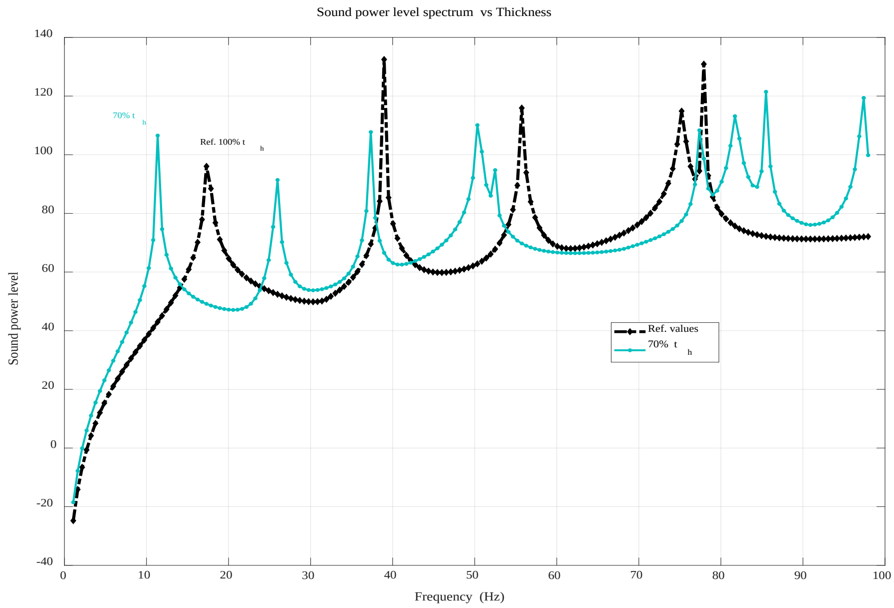

Fig. 13. Variation of the sound power level with the frequency for different values of the thickness

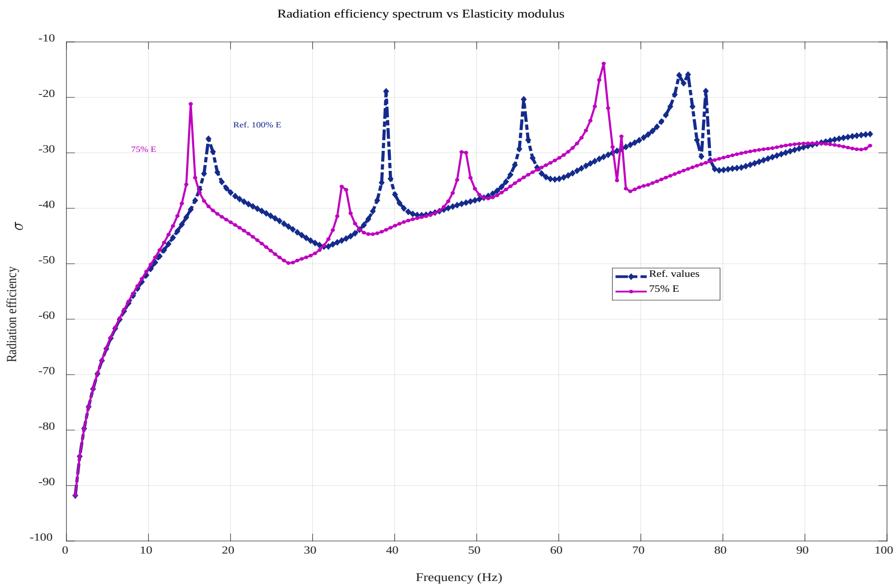

Fig. 14. Variation of the radiation efficiency with the frequency for different values of the elasticity modulus

Fig. 14 and 15 presents the variation of the radiation efficiency and the sound power level with the frequency for different values of the panel elasticity modulus. For lower rigidity value the resonant peaks are shifted to lower values of the frequency and the frequency interval between these peaks decrease slightly. The radiation efficiency and the sound power level for the fundamental frequency is higher as lower the value of the elasticity modulus.

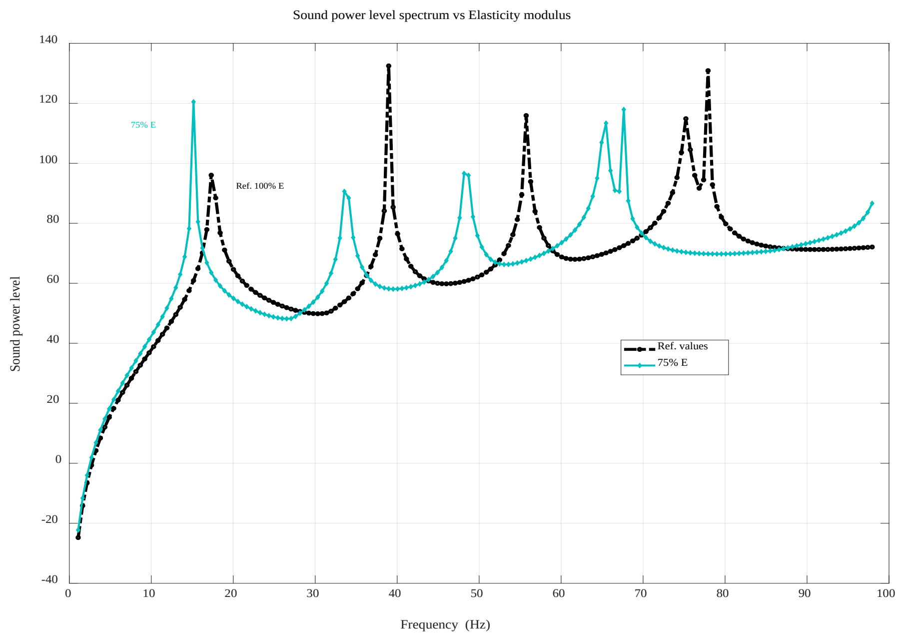

Fig. 15. Variation of the sound power level with the frequency for different values of the elasticity modulus

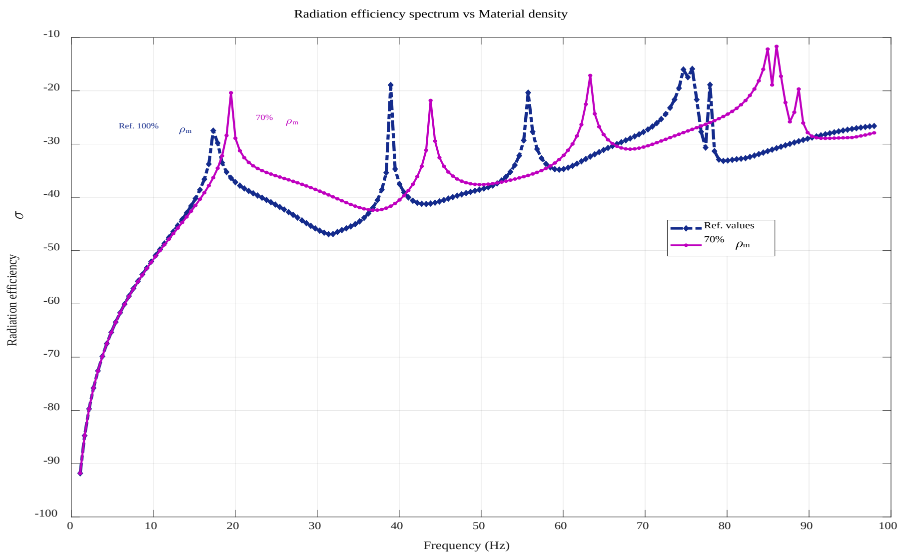

Fig. 16. Variation of the radiation efficiency with the frequency for different values of the material density

Fig. 16 and 17 presents the variation of the radiation efficiency and the sound power level with the frequency for different values of the panel material density. The resonant peaks are shifted to higher values of the frequency for the lighter material and the frequency interval between these peaks is slightly greater for the lower values of the material density. The radiation efficiency and the sound power level for the fundamental frequency are higher for the lighter material.

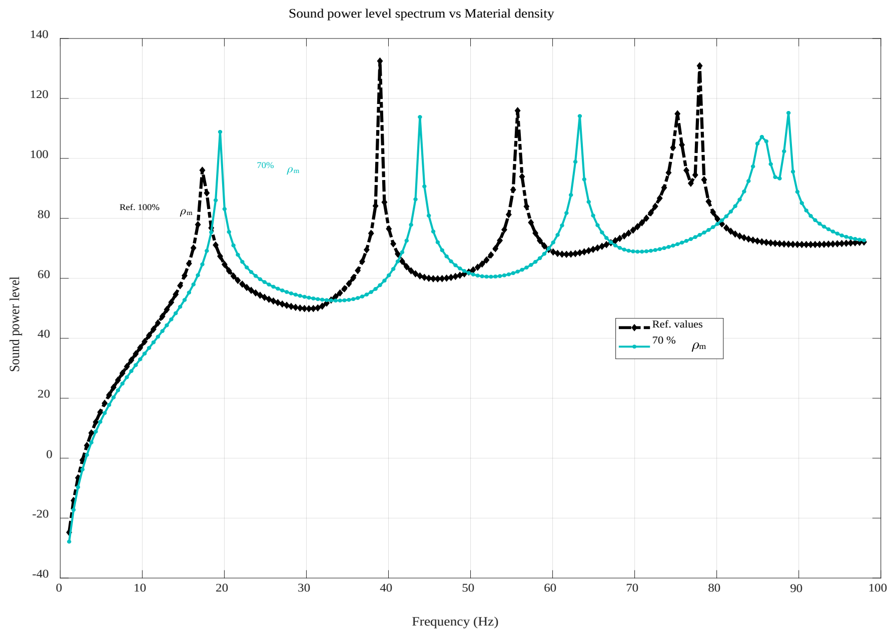

Fig. 17. Variation of the sound power level with the frequency for different values of the material density

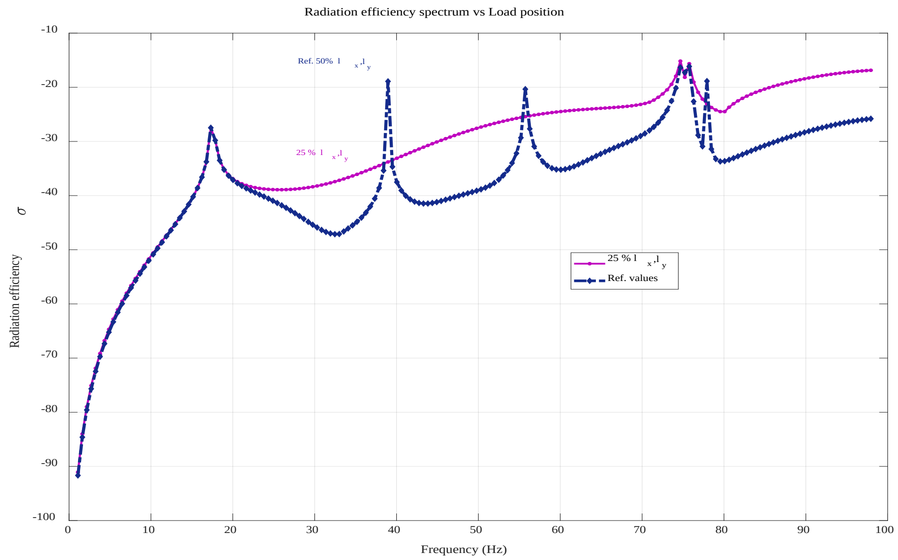

Fig. 18. Variation of the radiation efficiency with the frequency for different values of the load position

Fig. 18 and 19 presents the variation of the radiation efficiency and the sound power level with the frequency for different values of the excitation load position. When the load is applied at the 25% position, not all the resonant frequencies are excited as for the case of 50% position. The first and fourth resonant frequencies are excited and the values of the radiation efficiency and the sound power level coincides for the first or fundamental frequency and for the fourth resonant frequency

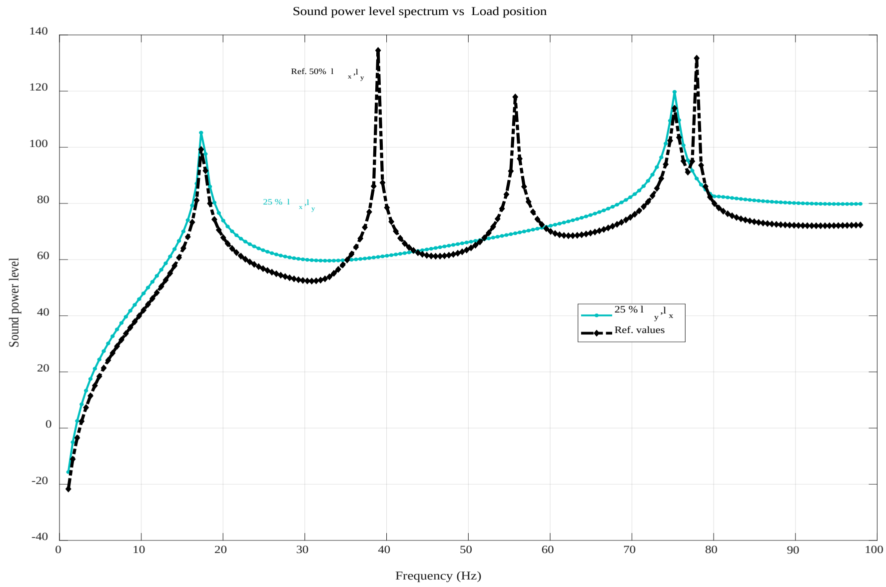

Fig. 19. Variation of the sound power level with the frequency for different values of the load position

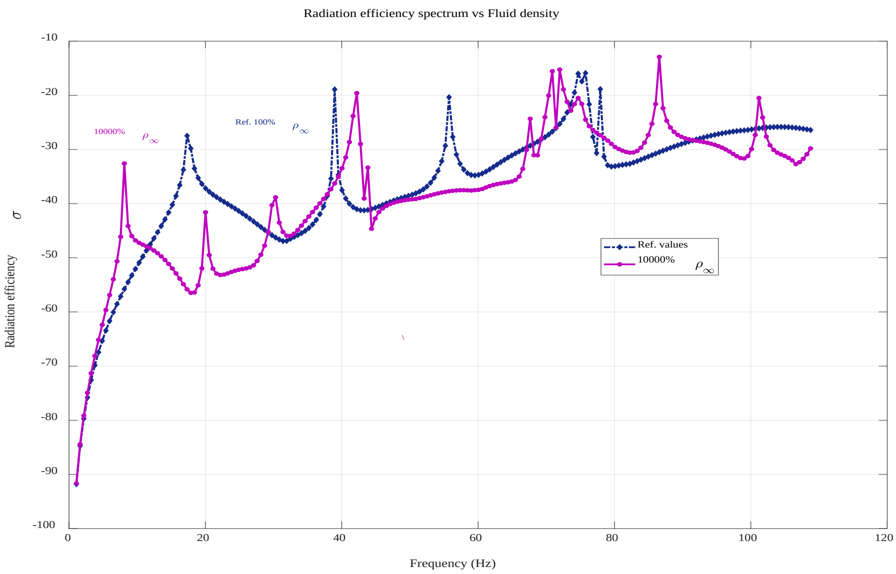

Fig. 20. Variation of the radiation efficiency with the frequency for different values of the fluid density

Fig. 20 and 21 presents the variation of the radiation efficiency and the sound power level with the frequency for different values of the fluid density. The resonant peaks are shifted to lower values of the frequency for the heavier fluid and the frequency interval between these peaks is greatly reduced for the higher value of the fluid density that is 100 times the reference value. The radiation efficiency is lower and the sound power level is higher for the fundamental frequency in the case of heavier fluid.

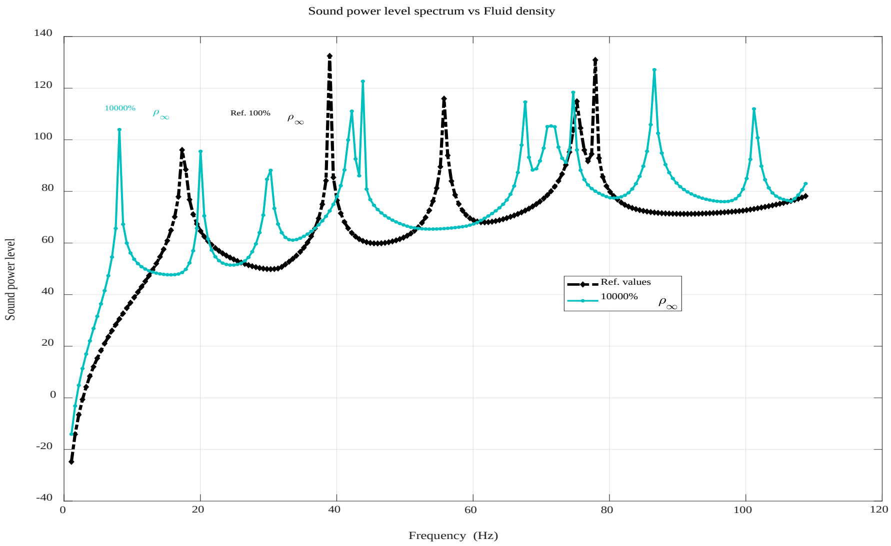

Fig. 21. Variation of the sound power level with the frequency for different values of the fluid density

Figs. 22, 23, 24, 25 and 26 presents the sound pressure level SPL directivity for different frequencies of the excitation load. The pressure of the field point x, y, z (averaged in the time period) is calculated at a distance of 10 m with respect to the center of the rectangular panel and in a plane perpendicular to the panel and parallel to the " x " direction. It is observed different shape configurations regarding the excitation frequency.

The directivity diagrams in all figures are symetric with respect to the vertical axes due to the center location of the excitation force. In general the number of lobes increase with the excitation frequency. In Figure 22 the maximum value of sound pressure is reached at vertical direction 90^0 and the diagram presents only one lobe. In the rest figures the maximum sound pressure level is reached very near of the 90^0 azimuthal position. In Figure 23 there is a main central lobe which is wider and of higher intensity than the two lateral lobes. In Figure 24 there is a main central lobe of higher intensity and lateral lobes of very small angular amplitude. In Figures 25 and 26 the number of main lobes increase with respect to the other figures of smaller excitation frequency. The reason is that for higher values of the excitation frequency, the influence of modal components of higher order is increased.

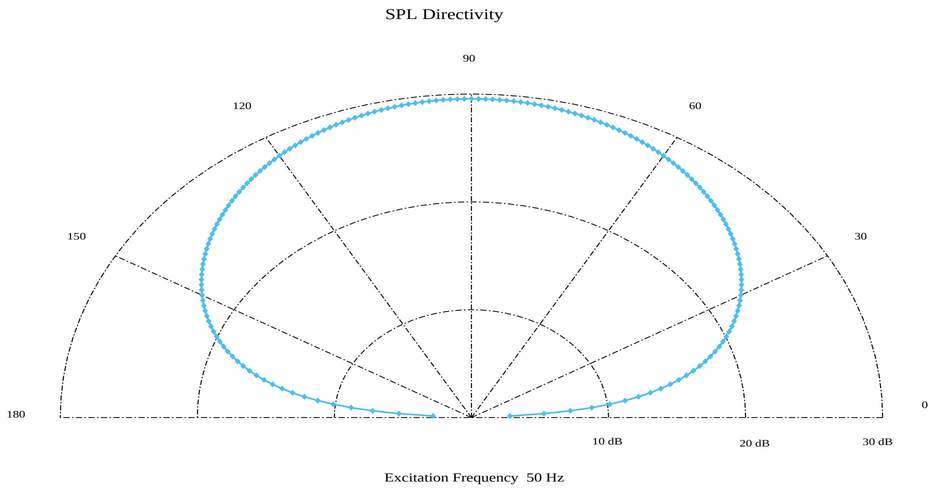

Fig. 22. Sound directivity of the panel for an excitation load of 50 Hz

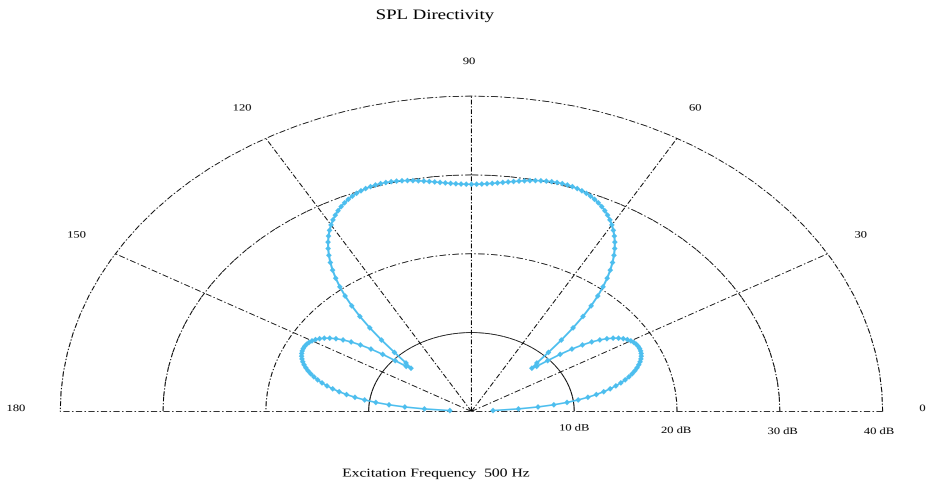

Fig. 23. Sound directivity of the panel for an excitation load of 500 Hz

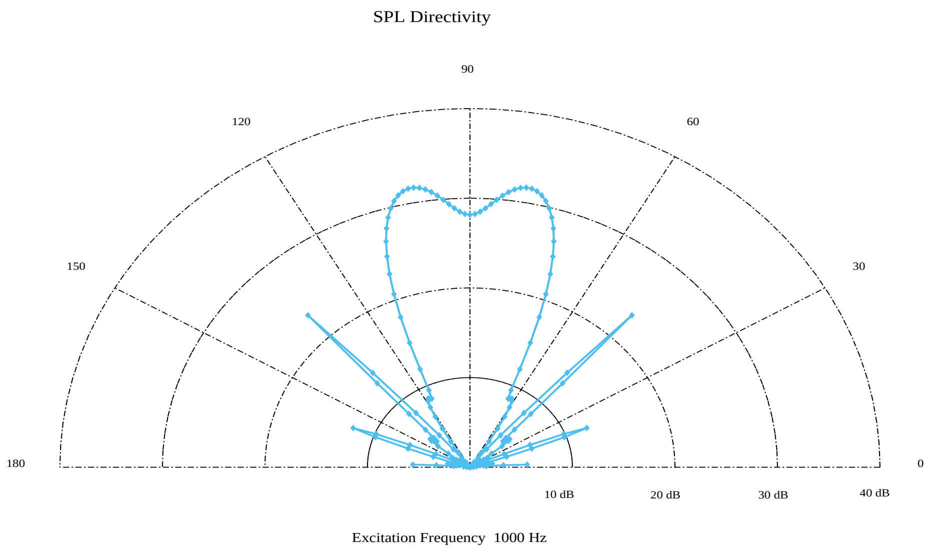

Fig. 24. Sound directivity of the panel for an excitation load of 1000 Hz

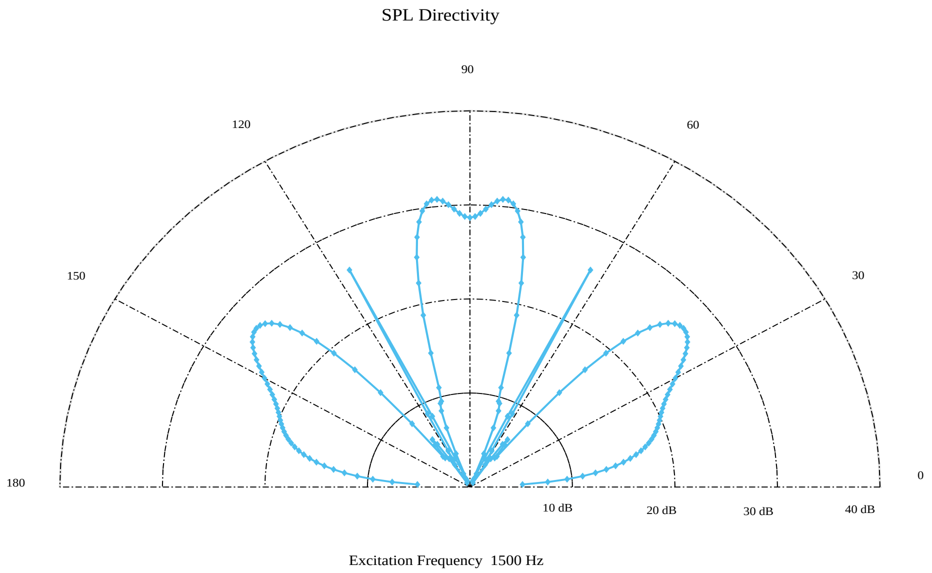

Fig. 25. Sound directivity of the panel for an excitation load of 1500 Hz

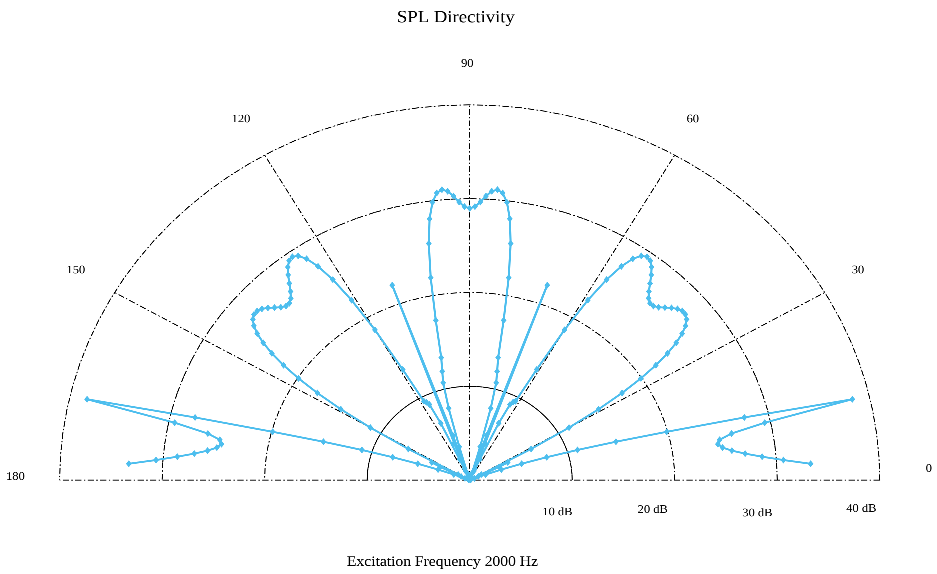

Fig. 26. Sound directivity of the panel for an excitation load of 2000 Hz

Thermal effects are considered in Figure 27 where it has been represented for en excitation frequency of 20 Hz the sound pressure directivity for two values of the panel temperature $\Theta = 0^0 C$ and $\Theta = 40^0 C$, both below the critical buckling temperature Θ_{cr} . The SPL decreases over the entire azimuthal range at higher temperature values. However for high values of the excitation frequency (1000 Hz or above), there is no dependence of the directivity with the panel temperature.

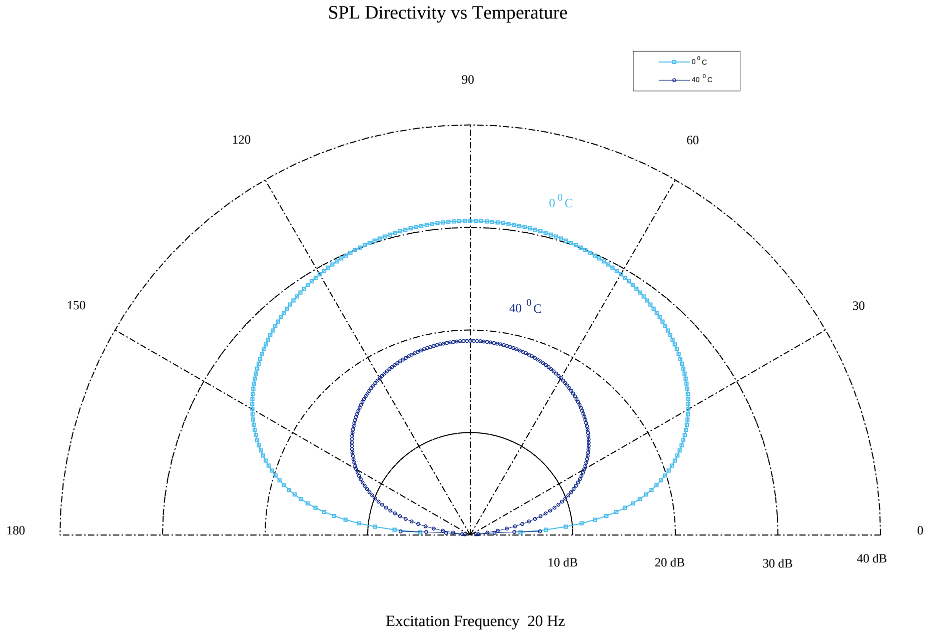

Fig. 27. Thermal effects on Sound directivity of the panel for an excitation load of 20 Hz

Table 2 presents various modal frequencies of the panel regarding its thermal condition for the cases of the panel in contact with fluid and in vacuum. The same results are obtained by Gascón-Pérez [25], so the validity of the present work.

Table 2. Free modal frequencies (Hz) of the reference panel in vacuum and with air for three thermal conditions

m , n	$f_v^{\Theta=0^0C}$	$f_a^{\Theta=0^0C}$	$f_v^{\Theta=20^0C}$	$f_a^{\Theta=20^{0C}}$	$f_v^{\Theta=40^0C}$	$f_a^{\Theta=40^0C}$
1 , 1	22.14	17.53	16.71	12.94	6.63	5.25
1 , 2	46.06	39.23	40.71	34.67	34.54	29.42
2 , 1	64.66	56.28	59.41	51.71	53.64	46.69
2 , 2	88.58	78.65	83.38	74.03	77.85	69.12

4. Conclusions

Acoustic radiation characteristics of a rectangular panel fully submerged in fluid and considering thermal effects has been analysed. Taking into account the equation of motion of the panel under an harmonic point excitation load and the acoustic pressure jump over the panel considering the K-H integral equation, the frequency response is obtained calculating the radiation efficiency and the sound power level spectrum expressed in logarithmic scale (dB).

Different parameters have been considered regarding this frequency response such as panel dimension, thickness, material density, fluid density, elasticity modulus, load position as well as panel temperature. In general, the influence of these parameters on the response frequency leads to the variation of the frequency of the resonant peaks and their amplitude, as well as variation of the frequency interval between these resonant peaks.

Furthermore it has been studied the acoustic radiation directivity expressed as a sound pressure level directivity of the panel for different frequencies of the excitation load, showing a great difference in the directivity configuration depending of the excitation frequency.

Finally, results are presented for different free frequencies of vibration of the panel in contact with fluid and in the vacuum case, considering different thermal loads.

The novelty of the present work is highlighted in the results obtained for a simply supported unbaffled rectangular panel where the thermoacoustic behaviour is analysed not only for the free vibration case as in [25], but for the forced vibration response where it has been made an study of the radiation characteristics such as acoustic power radiation and radiation efficiency frequency spectrum, as function of various geometrical and material parameters, characteristics of excitation load, and also considering different thermal loads, as well as the sound radiation directivity.

References

1. Atalla N, Nicolas J, Gauthier C. Acoustic radiation of an unbaffled vibrating plate with general elastic boundary conditions. The Journal of the Acoustical Society of America 1996; 99: 1484.
2. Laulagnet B. Sound radiation by a simply supported unbaffled plate. The Journal of the Acoustical Society of America 1998; 103: 2451.
3. Berry A et al. A general formulation for the sound radiation from rectangular baffled plates with arbitrary boundary conditions. The Journal of the Acoustical Society of America 1990; 88: 6.
4. Wilby JF. Aircraft interior noise. Journal of Sound and Vibration 1996; 190 (3): 545-564
5. Boley B, Barber A. Dynamic response of beams and plates to rapid heating. Journal of Applied Mechanics 1957; 24: 413-425.
6. Kim YW. Temperature dependent vibration analysis of functionally graded rectangular plates. Journal of Sound and Vibration 2005; 284 (3/5): 532-549.
7. Liu GR, Han X, Xu YG, Lam KY. Materials characterization of functionally graded material by means of elastic waves and a progressive learning neural network. Composites Science and Technology 2001; 61: 1401–1411
8. Iyer SR, Sinha SK and Schokker AJ. Ultrasonic C-scanimaging of post-tensioned concrete bridge structures for detection of corrosion andvoids. Computer-Aided Civil & Infrastructure Engineering 2005; 20: 79–94
9. Meo M, Polimeno U and Zumpano G. Detecting damage in composite materials using nonlinear elastic wave spectroscopy methods. Applied Composite Materials 2008;15: 115–126.
10. Maev RG. Acoustic Microscopy. Wiley-VCH,Weinheim 2008: 9–20.
11. Jeyaraj P, Ganesan N and Padmanabhan C. Vibration and acoustic response of a composite plate with inherent material damping in a thermal environment. Journal of Sound and Vibration 2009; 320: 322-338.
12. Geng Q and Li YM. Analysis of Dynamic and Acoustic Radiation Characters for a Flat plate under Thermal Environments. International Journal of Applied Mechanics 2012; 4 (3) 1250028: 1-16.
13. Chandra N et al. Vibro-acoustic response and sound transmission loss analysis of functionally graded plates. Journal of Sound and Vibration 2014; 333: 5786-5802
14. Yang T et al. Sound radiation of functionally graded materials plates in thermal environment. Composite Structures 2016; 144: 165-176
15. Li X and Yu K. Vibration and acoustic responses of composite and sandwich plates under thermal environment. Composite Structures 2015; 131: 1040-1049.
16. Li X, Yu K and Zhao R. Vibro-acoustic response of a clamped rectangular sandwich panel in thermal environment. Applied Acoustics 2017; 132: 82-96.
17. Liu Y and Li Y. Vibration and Acoustic Response of Rectangular Sandwich Plate under Thermal Environment. Shock and Vibration 2013; 20 (5): 1011-1030.
18. Sharma N, Mahapatra TR and Panda SK. Vibro-acoustic analysis of un-baffled curved composite panels with experimental validation. Structural Engineering & Mechanics 2017; 64 (1): 93-107.
19. Sharma N, Mahapatra TR and Panda SK. Numerical analysis of acoustic radiation responses of shear deformable laminated composite shell panel in hygrothermal environment. Journal of Sound and Vibration 2018; 431: 346-366.
20. Sharma N, Mahapatra TR and Panda SK. Numerical analysis of acoustic radiation properties Of laminated composite flat panel in thermal environment: A higher-order finite-boundary element approach. Proceedings of the Institution of Mechanical Engineer, Part C: Journal of Mechanical Engineering Sciences 2018
21. Cao S, Lee HP and Lim KM. Estimation of Wave Reflection Coefficient by Semi-Analytical Method in an Acoustic Black Hole Beam. International Journal of Applied Mechanics 2020; 12 (1): 20510004.
22. Kumar S and Lee HP. Recent Advances in Active Acoustic Metamaterials. International Journal of Applied Mechanics 2019; 11 (8): 1950081.
23. Sobhy M. An accurate shear deformation theory for vibration and buckling of FGM sandwich plates in hygrothermal environment. International Journal of Mechanical Sciences 2016; 110: 62-77.

24. Zhou K, Huang X, Tian J and Hua H. Vibration and flutter analysis of supersonic porous functionally graded material plates with temperature gradient and resting on elastic foundation. Composite Structures 2018; 204: 63-79.
25. Gascón-Pérez M. Thermo-Acoustic Effects on the Natural Frequencies of Vibration of an Elastic Rectangular Panel. International Journal of Applied Mechanics 2021; 13 (2): 2150019 1-18
26. Wang CY & Wang CM. Structural vibration: exact solutions for strings, membranes, beams and plates. 2014; (CRC Press, Boca Raton FL).
27. Boley BA and Weiner JH. Theory of Thermal Stresses. 1997; (Dover Publications, Mineola NY).
28. Junger MC and Feit D. Sound, Structures and Their Interaction. 1972; (M.I.T. Press,London).
29. Crocker MJ. Handbook of noise and vibration control. 2007; (John Wiley & Sons, New Jersey).
30. Fahy F. The foundations of engineering acoustics. 2001; (Elsevier Academic Press, London).
31. Roussos IM. Improper Riemann integrals. 2014; (CRC Press, Boca Raton FL).
32. Gascón-Pérez M. Interactions of an oscillating rectangular membrane with a compressible Fluid. International Journal of Applied Mechanics 2018; 10 (2): 1850016 , 1-13.
33. Kwak MK. Hydroelastic Vibration of Rectangular Plates. Journal of Applied mechanics 1996; 63: 110-115.
34. Li S and Li X. The effects of distributed masses on acoustic radiation behavior of plates. Applied Acoustics 2008; 69: 272–279